Journal of Innovative Optical Health Sciences
Vol. 8, No. 3 (2015) 1541005 (10 pages)

DOI: 10.1142/S1793545815410059

Multi-layered tissue head phantoms for noninvasive optical diagnostics

M. S. Wróbel*,¶, A. P. Popov†, A. V. Bykov†, M. Kinnunen†,
M. Jędrzejewska-Szczerska* and V. V. Tuchin†,‡,§

*Department of Metrology and Optoelectronics
Gdańsk University of Technology
Gabriela Narutowicza Street 11/12
80-233 Gdańsk, Poland

†Optoelectronics and Measurement Techniques Laboratory
Faculty of Information Technology and Electrical Engineering
University of Oulu, P. O. Box 4500
FI-90014 Oulu, Finland

‡Research-Educational Institute of Optics and Biophotonics
Saratov State University, Saratov 410012, Russia

§Institute of Precise Mechanics and Control
Russian Academy of Sciences, Saratov 410028, Russia
¶maciejswrobel@gmail.com

Received 3 March 2014
Accepted 17 June 2014
Published 18 July 2014

Extensive research in the area of optical sensing for medical diagnostics requires development of tissue phantoms with optical properties similar to those of living human tissues. Development and improvement of *in vivo* optical measurement systems requires the use of stable tissue phantoms with known characteristics, which are mainly used for calibration of such systems and testing their performance over time. Optical and mechanical properties of phantoms depend on their purpose. Nevertheless, they must accurately simulate specific tissues they are supposed to mimic. Many tissues and organs including head possess a multi-layered structure, with specific optical properties of each layer. However, such a structure is not always addressed in the present-day phantoms. In this paper, we focus on the development of a plain-parallel multi-layered phantom with optical properties (reduced scattering coefficient μ_s' and absorption coefficient μ_a) corresponding to the human head layers, such as skin, skull, and gray and white matter of the brain tissue. The phantom is intended for use in noninvasive diffuse near-infrared spectroscopy (NIRS) of human brain. Optical parameters of the fabricated phantoms are reconstructed using spectrophotometry and inverse adding-doubling calculation method. The results show that polyvinyl chloride-plastisol (PVCP) and zinc oxide (ZnO) nanoparticles are suitable materials for fabrication of tissue mimicking phantoms with controlled scattering properties. Good matching

was found between optical properties of phantoms and the corresponding values found in the literature.

Keywords: Tissue-mimicking phantoms; optical properties; near-infrared spectroscopy; head model.

1. Introduction

Noninvasive diagnostics is aimed to provide information about internal parameters of living subjects, which may revolutionize medical diagnostics. Thus it is extensively studied for the purposes such as disease detection, oximetry, hemodynamics, or imaging. A diffuse near infrared spectroscopy (NIRS) is one of such methods.[1] It utilizes several optical wavelengths to monitor parameters of tissues such as oxygen saturation, changes in blood volume, blood flow and muscle O_2. Such optical measurement systems for biomedical applications rely on tissue-equivalent phantoms for testing system design and comparing different measurement methods.[2–9] Use of real human tissues is impractical since the optical properties of such samples change in various atmospheric conditions (i.e., humidity, temperature) and rapidly degrade over time, thus they are unusable as standards with known and stable properties. Therefore, optical properties of phantoms (scattering coefficient μ_s, absorption coefficient μ_a, scattering anisotropy factor g, refractive index n, and thickness L) should be properly tuned to correspond to that of tissues they mimic. Properties of phantoms differ depending on the purpose they are designed for, as various noninvasive optical diagnostic techniques utilize phantoms.[5–14] The geometry of the head-mimicking phantoms used previously is not complex being either in a form of a slab,[15] a cylinder,[16] a container,[17] a plastic skull.[18] Phantoms with more sophisticated geometry simulating a head shape and the brain are under developed.[19] The structure of optical phantoms usually comprises three parts.[5,6,20] First, the matrix material, which is chosen with regards to its mechanical properties, refractive index, and stability over time. Another constituent, the scattering component, is used to affect scattering properties of the phantom. Scattering depends on the particle refractive index and size distribution. Most common scatterers are TiO_2 nanoparticles,[5,6,11] plastic microspheres,[5,21,22] or lipids.[23–25] To affect absorption, absorbing agents such as ink, whole blood,[26] or dyes[21] are used.

This paper is based on the previous research carried out by our group[27] where the fiber-based NIRS system, designed for use during functional magnetic resonance imaging (fMRI), utilized phantoms for sensing purpose. These preliminary results were very promising when comparison between the *in vivo* (forehead location) and the multi-layered phantom was performed at two wavelengths (830 nm and 905 nm), even though the phantom layers were prepared to match the optical properties of the real tissue at 900 nm only. The attenuation of the light at different source-detector separations were in excellent agreement with Monte Carlo simulations. However, at a current state of research, significant discrepancies between theoretical investigations and real measurements were evident. Thus, this paper is exclusively focused on the process of developing precise tissue-mimicking layered phantoms, with an emphasis on calculating proper quantities of nanoparticles to affect the scattering, as well as measuring optical properties of the manufactured phantoms. We present a multi-layered phantom of head model tissue layers representing skin, skull, cerebrospinal fluid (CSF), and two distinct brain tissues: gray and white matter. All the layers of the presented phantom (besides CSF) were fabricated using polyvinyl chloride-plastisol (PVCP) as a matrix material and zinc oxide (ZnO) nanoparticles as a scattering agent. The CSF-mimicking layer was made from silicone to form an extremely transparent object. This phantom is intended for further research focused on testing and optimizing NIRS method.[27–29] We will use it for the application of diffuse NIRS operating at 805–905-nm wavelengths for monitoring brain activity. Consequently, the optical properties are tuned to correspond to those of the head specifically at this spectral range, with behavior at other wavelengths showed for comparison.

2. Materials and Methods

Optical properties of head model tissue layers (Table 1) were taken from the literature.[29–35] Since

Table 1. Reduced scattering coefficients, absorption, and thicknesses of head-mimicking phantom layers corresponding to real tissue layers at 915-nm wavelength.

Tissue	μ_s' [mm^{-1}]	μ_a [mm^{-1}]	g	Thickness L [mm]	References
Skin	1.44	0.05	0.88	3	31, 33
Skull	1.5	0.04	0.94	10	32
CSF	0.0001	0.001	0.999	2	30
Gray matter	2.40	0.03	0.96	4	34
White matter	7.80	0.01	0.87	20	35

the intended purpose of the phantom is NIRS of brain, only the knowledge of the absorption coefficient μ_a and the reduced scattering coefficient μ_s' is required for the diffuse regime of light propagation realized in the case of head.[5,28–30] The following equation is used to calculate the reduced scattering coefficient[36–38]:

$$\mu_s' = \mu_s(1-g), \tag{1}$$

where μ_s is a scattering coefficient and g is a scattering anisotropy factor.

In order to match the reduced scattering coefficient of fabricated phantoms to those of tissues, it was necessary to calculate the required concentrations of zinc oxide (ZnO) nanoparticles according to the Mie theory of scattering. First, we calculated g-factors and the scattering efficiency factors Q_s for different ZnO particle sizes (Fig. 1) and predicted the resulting g_Σ value accounting for the ZnO particle size distribution (theoretical $g_\Sigma = 0.76$). The scattering efficiency factor is defined as a ratio between the scattering cross section σ_s and the geometrical cross section σ_g: $Q_s = \sigma_s/\sigma_g$. Then, we fabricated and measured PVCP phantoms without particles and with low particle concentration (1.5 mg/mL), so that only single scattering occurs to retrieve g_Σ value experimentally ($g_\Sigma = 0.80$). Knowing particles size distribution, concentration N, scattering efficiency Q_s (Fig. 1), and accounting for the fact that $\mu_s = \sigma_s N$, we estimated the required concentration of ZnO particles to match real μ_s'. Since g of the real head tissues is larger than the obtained theoretical parameters of the phantom, we focus on μ_s' calculated to match μ_s' of the phantom and that of a tissue because we apply our phantoms for NIRS. Absorption property of the intrinsic matrix of PVCP was used, slightly surpassing the values for real head layers.

The matrix material used for phantom fabrication was PVCP (M-F Manufacturing Co., Fort Worth, TX, USA), which becomes transparent due to polymerization after heating at high temperature. Zinc oxide powder (Sigma-Aldrich, Germany) with an average particle size of 0.34 μm (Fig. 2) was used as a scattering agent to obtain desired optical properties. PVCP was thoroughly mixed with ZnO to ensure homogenous distribution. The mixture was sonicated for 15 min to destroy clusters and evenly distribute the particles in the suspension. It was then poured into plane rectangular molds and heated for 1 h at 180°C.

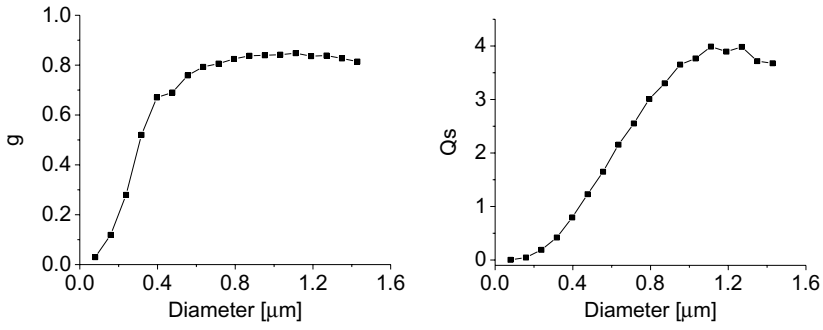

(a) (b)

Fig. 1. g-factor (a), and scattering efficiency factor Q_s (b), calculated for individual ZnO particles of different sizes used for phantom fabrication. The calculations are based on the Mie theory of scattering. Theoretical and experimental values of g_Σ correspond to the actual ZnO powder used for phantom fabrication and the size distribution is taken into account of the particles: $g_\Sigma = 0.76$ (theory), $g_\Sigma = 0.80$ (experiment).

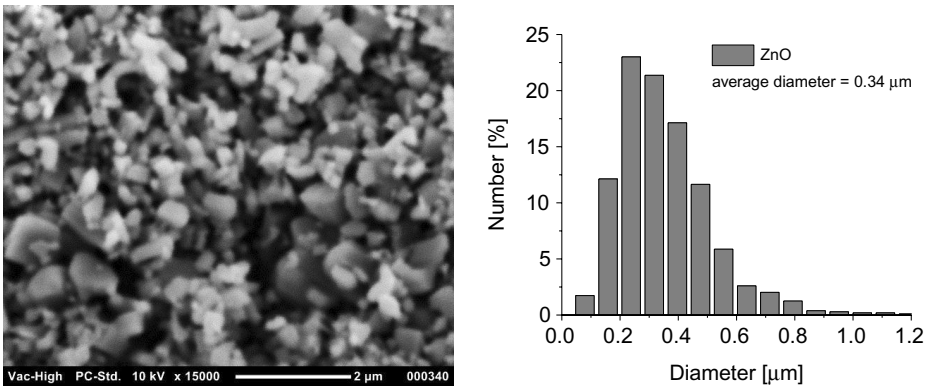

(a) (b)

Fig. 2. Scanning electron microscopy (SEM) image (a) and size distribution (b) of the used ZnO particles.

3. Results

A series of 0.5-mm-thick plain layers mimicking skin, skull, gray, and white matter by their optical (but not geometrical) properties, with pre-calculated ZnO concentrations were manufactured. Total reflectance, total transmittance, and collimated transmittance were measured (Fig. 3) using OL-750 spectrophotometer system (Optronic Laboratories, USA) with a Si high-sensitivity detector module OL 750-HSD-300 (wavelength 0.25–1.1 μm) and integrating spheres; the latter was used to account for scattering properties of the samples. The refractive index was measured [Fig. 3(a)] using a DR-M2/1550(A) multi-wavelength Abbe refractometer (Atago, Japan). Spectral-domain Optical Coherence Tomography system Hyperion (Thorlabs, USA) was used to

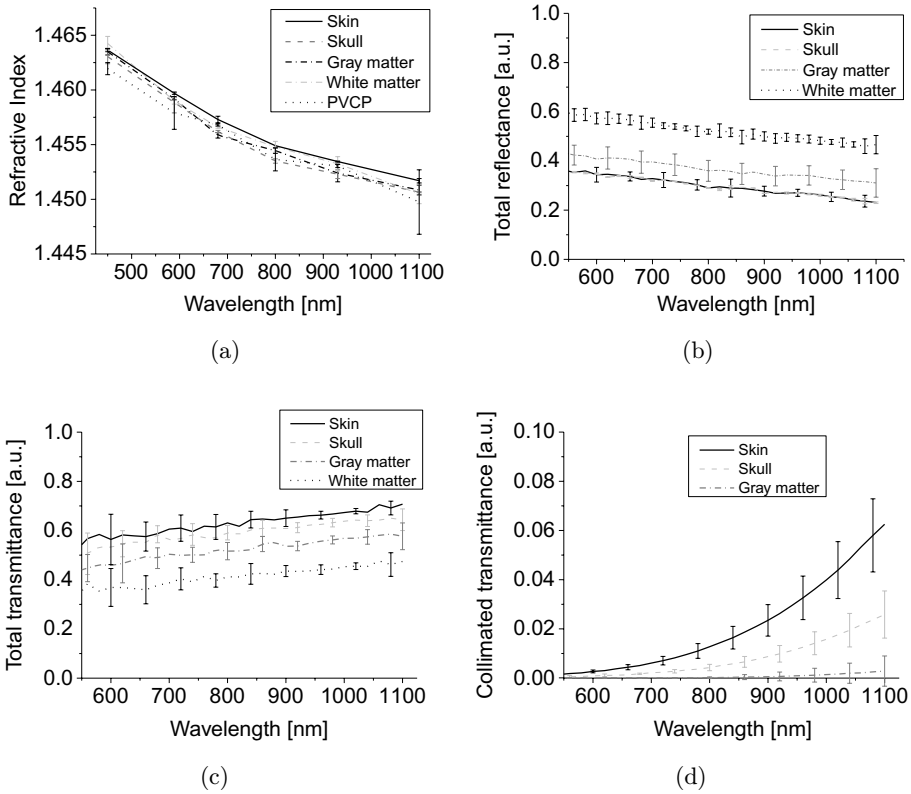

(a) (b) (c) (d)

Fig. 3. Measured refractive index (a), total reflectance (b), total transmittance (c), and collimated transmittance (d), as input (along with thickness) for inverse adding-doubling algorithms.

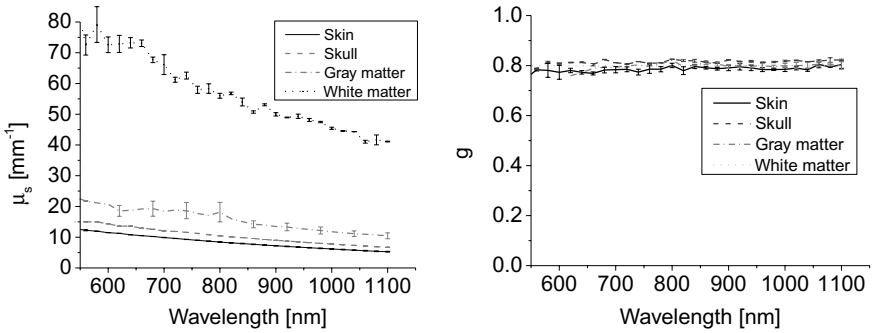

(a) (b)

Fig. 4. Reconstructed optical properties: scattering coefficient (a) decreases linearly with wavelength; anisotropy factor g and (b) remains constant ($g = 0.8$) for the whole spectral range. For the white matter phantom, g was calculated to be 0.8 based on additional measurements of thinner samples.

confirm the refractive index measurements at 930-nm wavelength. Thickness L of the phantoms was also measured using OCT (resolution in air: 5.8 μm). The optical properties of phantoms (μ_s and g) were then reconstructed using inverse adding-doubling algorithms[36–40] (Fig. 4). Refractive index of the phantoms was measured twice and the spectrophotometer measurements were repeated three times on several sites over each phantom (two phantoms for each set of properties). Standard deviation in Figs. 3–5 is defined from the measurements averaged over the whole set of measurements.

Differences in the refractive index (Fig. 3) of phantoms with different concentrations of ZnO are smaller than the measurement errors. Therefore, no reliable differences in the refractive index were

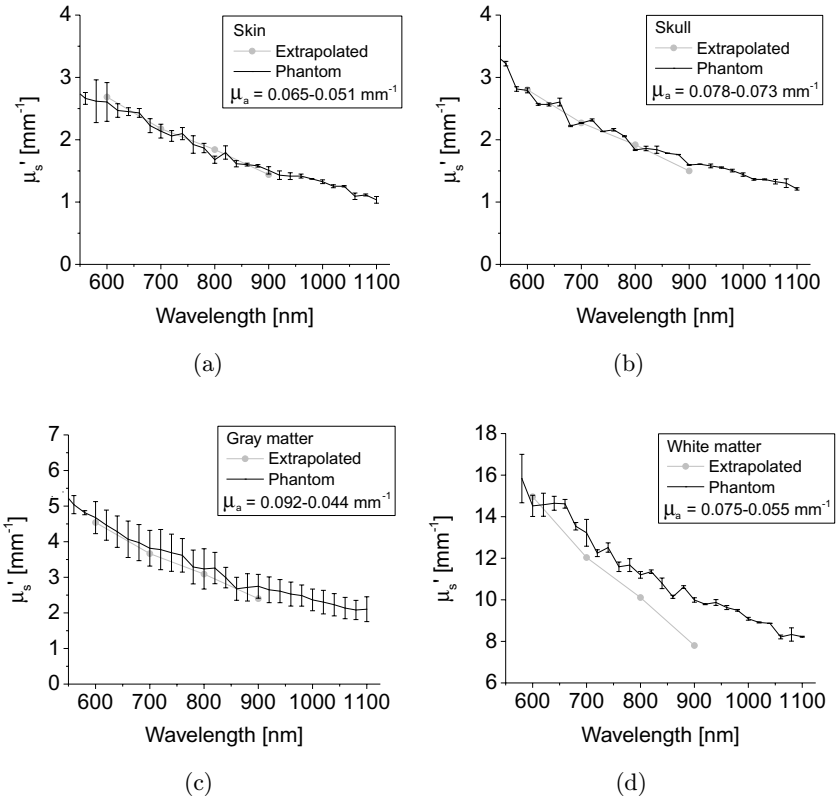

(a) (b)

(c) (d)

Fig. 5. Reduced scattering coefficients of the head-mimicking layers. Linear extrapolation based on the single-scattering phantom measured at 900-nm wavelength ("Extrapolated"), and results of measurements of the fabricated phantoms, simulating skin (a), skull (b), gray matter (c), and white matter (d).

observed due to limited accuracy of measurement methods. Spectrophotometric measurements show clear distinction between the phantom layers. The absorption coefficient depends on the phantom layer and changes slightly within $\mu_a = 0.044 - 0.092\,\mathrm{mm}^{-1}$; the g-factor remains the same ($g = 0.8$) for all phantoms for the whole spectrum. Since collimated transmittance could not be measured for the 0.5 mm-thick white matter phantom layer, the value for $g = 0.8$ was used based on measurements of thinner phantoms. Scattering properties of different head-mimicking layers differ, which is clearly demonstrated by Fig. 5.

Reconstructed reduced scattering coefficient of the phantom (Fig. 5) is in good agreement with the linear extrapolation of the single-scattering phantom properties and matches with those of real tissue layers. Therefore, the presented calculations, the fabrication method, and the measurements of tissue-mimicking phantom layers are correct. Errors arise from a series of factors, such as: inhomogeneous mixing of ZnO particles with PVCP, clustering of particles due to insufficient sonication of the mixture, and particle sedimentation. Especially in higher concentrations, the nanoparticles are difficult to mix properly and they quickly sink to the bottom of the mold, before PVCP solidifies. This makes phantoms inhomogeneous, thus uncontrollably changing the phantoms' optical properties.

4. Discussion

Accurate matching of optical properties by phantom relies on the choice of materials used for their fabrication. While matching the absorption coefficient of phantoms can be simply achieved by addition of a specific concentration of substances which absorb light at required spectral range, accurately matching the scattering properties is still a major challenge. Several manufacturing techniques have been so far employed for this purpose.[5,6,20,22,41] One of them, used for liquid phantoms, is the use of aqueous intralipid suspensions of a certain concentration. We previously employed such phantoms for glucose sensing employing OCT, photoacoustics, and time-of-flight techniques.[42–45] This fat emulsion substance has known and reproducible scattering coefficients due to its uniform fabrication procedure.[46,47] However liquid samples cannot be formed in desired shapes and are unsuitable for long-term use; thus solid phantoms should be elaborated. Such phantoms are made commonly using nanoparticles of controlled size distribution suspended in a matrix material. Careful choice of matrix material and scattering nanoparticles is the basis for phantom manufacturing using this approach, which was also employed in this paper. Scattering particles differ in their size, shape, refractive index, and absorption spectrum which affect the scattering coefficient and anisotropy of the particles. We have used ZnO nanoparticles due to their higher anisotropy factor ($g = 0.8$ as presented in Fig. 1), which is much closer to that of real human tissues than TiO_2 particles.[10,11] As an ultimate goal, we aim at making phantoms having all three parameters (scattering and absorption coefficients, and a scattering anisotropy factor) matching those of relevant tissue (head-mimicking layers) and potentially versatile (suitable for any kind of optical technique). Despite the commonly used diffuse regime of light propagation, where only reduced scattering and absorption coefficients are needed to be taken into account, biotissue-mimicking phantoms for optical coherence tomography, where scattering anisotropy (g-factor) is important, possess irrelevant g-factor values and not discussed at all.[48,49] In these papers, the used particles of sub-micron size, thus resulting in a relatively small g-factor value, much lower than that of the biological tissues (0.9 or larger[31]). With our choice of ZnO particles we managed to get the g-factor as large as 0.80. However, since we focus on the diffusion regime in this particular technique, NIRS, it is sufficient to have only two values (reduced scattering and absorption coefficients) close to those of head-mimicking tissue layers.

Some studies employed the use of actual human bones when the systems they were designed for required the simulation of bones.[50,51] This approach has several disadvantages, which limit their potential use. First, in real situation, the bones are wet while inside the body. Bones changes their optical properties significantly and uncontrollably when dried, which is unacceptable for most applications. The stability of phantom properties over time is also an important factor. Thus, using real tissues as phantoms is often unreliable due to their degradation. Moreover, the use of actual bones prohibits one from controlling their thickness and their optical properties, which are different when dealing with child or adult bones and differ among people.

Phantoms presented here are 0.5 mm-thick. In case of greater thickness and higher absorption and

scattering coefficients, light is strongly attenuated, which prohibits the measurements of collimated transmittance of such samples. In order to characterize all the scattering properties of the materials $(\mu_a, \mu_s, \mu'_s, g)$, lack of collimated transmittance measurements makes retrieval of the anisotropy factor impossible, and consequently the μ_s. We focus on a single wavelength of the near-infrared spectrum, as a representative of the radiation spectrum used in our NIRS system.[27] As our preliminary tests showed, the phantoms look promising for the 830-nm radiation and also in the NIRS system. And we used an even more extended spectral range to see how the phantom optical properties match those of the values of real head layers. While characterizing the phantoms with the thickness of real tissues and specific geometry, which reflects real tissue morphology, not all optical properties can be measured. This is a crucial factor that has to be taken into account with the development of phantoms. Several technical difficulties are associated with fabrication of phantoms using nanoparticles, such as: sedimentation, clustering, and inhomogeneous mixing of nanoparticles. This is mostly evident while phantoms are made in larger volumes or in intricate shapes. That is why a controlled manufacturing procedure based on precise calculations of required nanoparticles concentrations was employed, with the possibility of creating thicker phantoms from stacked smaller layers with known optical properties. When the materials with suitable optical properties are obtained, the real shapes of the head-mimicking layers would be of high importance, even though other studies show little dependence of brain morphological structure on light propagation.[30] In this case, magnetic resonance imaging (MRI) data can be used in combination either with mechanical fabrication or 3D printing of molds.

In conclusion, we tested our phantoms for their stability, which should surpass that of the liquid phantoms. Our data show that the optical properties were stable at least for four months of storage in light-protecting conditions (UV and blue light component induce formation of free radicals[52,53] that can change optical properties of phantoms).

5. Conclusion

We have produced phantom layers mimicking head layers such as skin, skull, gray, and white matter with controlled optical properties. PVCP was used as a matrix material and zinc oxide as a scattering agent. The desired concentrations were based on measurements of single-scattering PVCP with ZnO phantom, compared with PVCP and extrapolated. The optical properties of phantoms were measured using a spectrophotometer and calculated using inverse adding-doubling algorithms. Produced phantom layers proved the extrapolation calculations, with properties matching those of real tissues at 915-nm wavelength, as intended. The phantoms will be used for testing and development of our laboratory in-house made NIRS measurement system, and the measured optical properties will be used for Monte Carlo simulations of light propagation in multi-layered head model to optimize measurement geometry.

Acknowledgments

This study was partially supported by: the National Science Center, Poland funding allocated on the basis of the decision number DEC-20011/03/D/ST7/03540; Foundation for Polish Science under Grant No. 173/UD/SKILLS/2012; DS Programs of the Faculty of Electronics, Telecommunications and Informatics, Gdańsk University of Technology; European Cooperation in Science and Technology (COST) Action BM1205; FiDiPro project 40111/11, TEKES (Finnish Funding Agency for Technology and Innovation); Government of the Russian Federation (Grant No. 14.Z50.31.0004 to support scientific research projects implemented under the supervision of leading scientists) and Russian Presidential grant NSh-703.2014.2.

References

1. M. Ferrari, L. Mottola, V. Quaresima, "Principles, techniques, and limitations of near infrared spectroscopy," *Can. J. Appl. Physiol. Rev. Can. Physiol. Appliquée* **29**, 463–487 (2004).
2. M. L. Clarke, J. Y. Lee, D. V. Samarov, D. W. Allen, M. Litorja, R. Nossal, J. Hwang, "Designing microarray phantoms for hyperspectral imaging validation," *Biomed. Opt. Express* **3**, 1291–1299 (2012).
3. R. X. Xu, K. Huang, R. Qin, J. Huang, J. S. Xu, L. Ding, U. S. Gnyawali, G. M. Gordillo, S. C. Gnyawali, C. K. Sen, "Dual-mode imaging of cutaneous tissue oxygenation and vascular function," *J. Vis. Exp.* **46**, e2095 (2010).

4. J. Hwang, J. C. Ramella-Roman, R. Nordstrom, "Introduction: Feature issue on phantoms for the performance evaluation and validation of optical medical imaging devices," *Biomed. Opt. Express* **3**, 1399–1403 (2012).
5. B. W. Pogue, M. S. Patterson, "Review of tissue simulating phantoms for optical spectroscopy, imaging and dosimetry," *J. Biomed. Opt.* **11**, 041102 (2006).
6. G. Lamouche *et al.*, "Review of tissue simulating phantoms with controllable optical, mechanical and structural properties for use in optical coherence tomography," *Biomed. Opt. Express* **3**, 1381–1398 (2012).
7. T. T. Nguyen, H. N. Le, M. Vo, Z. Wang, L. Luu, J. C. Ramella-Roman, "Three-dimensional phantoms for curvature correction in spatial frequency domain imaging," *Biomed. Opt. Express* **3**, 1200–1214 (2012).
8. A. E. Cerussi, R. Warren, B. Hill, D. Roblyer, A. Leproux, A. F. Durkin, T. D. O'Sullivan, S. Keene, H. Haghany, T. Quang, "Tissue phantoms in multicenter clinical trials for diffuse optical technologies," *Biomed. Opt. Express* **3**, 966–971 (2012).
9. J. R. Cook, R. R. Bouchard, S. Y. Emelianov, "Tissue-mimicking phantoms for photoacoustic and ultrasonic imaging," *Biomed. Opt. Express* **2**, 3193–3206 (2011).
10. A. V. Bykov, A. P. Popov, M. Kinnunen, T. Prykäri, A. V. Priezzhev, R. Myllylä, "Skin phantoms with realistic vessel structure for OCT measurements," *Proc. SPIE* **7376**, 73760F (2010).
11. A. V. Bykov, A. P. Popov, A. V. Priezzhev, R. Myllyla, "Multilayer tissue phantoms with embedded capillary system for OCT and DOCT imaging," *Proc. SPIE* **8091**, 80911R (2011).
12. A. Agrawal, M. Connors, A. Beylin, C.-P. Liang, D. Barton, Y. Chen, R. A. Drezek, T. J. Pfefer, "Characterizing the point spread function of retinal OCT devices with a model eye-based phantom," *Biomed. Opt. Express* **3**, 1116–1126 (2012).
13. L. Luu, P. A. Roman, S. A. Mathews, J. C. Ramella-Roman, "Microfluidics based phantoms of superficial vascular network," *Biomed. Opt. Express* **3**, 1350–1364 (2012).
14. S. L. Jacques, B. Wang, R. Samatham, "Reflectance confocal microscopy of optical phantoms," *Biomed. Opt. Express* **3**, 1162–1172 (2012).
15. A. J. Macnab, R. E. Gagnon, "Phantom testing of two clinical spatially-resolved NIRS instruments," *J. Spectrosc.* **19**, 165–169 (2005).
16. R. J. Cooper, R. Eames, J. Brunker, L. C. Enfield, A. P. Gibson, J. C. Hebden, "A tissue equivalent phantom for simultaneous near-infrared optical tomography and EEG," *Biomed. Opt. Express* **1**, 425–430 (2010).
17. D. K. Joseph, T. J. Huppert, M. A. Franceschini, D. A. Boas, "Diffuse optical tomography system to image brain activation with improved spatial resolution and validation with functional magnetic resonance imaging," *Appl. Opt.* **45**, 8142–8151 (2006).
18. R. L. Barbour, R. Ansari, R. Al Abdi, H. L. Graber, M. B. Levin, Y. Pei, C. H. Schmitz, Y. Xu, "Validation of near infrared spectroscopic (NIRS) imaging using programmable phantoms," *Proc. SPIE* **6870**, 687002–10 (2008).
19. R. L. Barbour, H. L. Graber, Y. Xu, Y. Pei, C. H. Schmitz, D. S. Pfeil, A. Tyagi, R. Andronica, D. C. Lee, S.-L. S. Barbour, J. D. Nichols, M. E. Pflieger, "A programmable laboratory testbed in support of evaluation of functional brain activation and connectivity," *IEEE Trans. Neural Syst. Rehabil. Eng. Publ. IEEE Eng. Med. Biol. Soc.* **20**, 170–183 (2012).
20. D. D. Royston, R. S. Poston, S. A. Prahl, "Optical properties of scattering and absorbing materials used in the development of optical phantoms at 1064 nm," *J. Biomed. Opt.* **1**, 110–116 (1996).
21. D. V. Samarov, M. L. Clarke, J. Y. Lee, D. W. Allen, M. Litorja, J. Hwang, "Algorithm validation using multicolor phantoms," *Biomed. Opt. Express* **3**, 1300–1311 (2012).
22. R. C. Chang, P. Johnson, C. M. Stafford, J. Hwang, "Fabrication and characterization of a multilayered optical tissue model with embedded scattering microspheres in polymeric materials," *Biomed. Opt. Express* **3**, 1326 (2012).
23. V. Kodach, N. Bosschaart, J. Kalkman, T. G. van Leeuwen, D. J. Faber, "Concentration dependent scattering coefficients of intralipid measured with OCT," *Biomedical Optics 3-D Imaging*, OSA Technical Digest (CD), paper BSuD11, Optical Society of America (2010).
24. P. I. Rowe, R. Künnemeyer, A. McGlone, S. Talele, P. Martinsen, R. Oliver, "Thermal stability of intralipid optical phantoms," *Appl. Spectrosc.* **67**, 993–996 (2013).
25. S. C. Kanick *et al.*, "Scattering phase function spectrum makes reflectance spectrum measured from Intralipid phantoms and tissue sensitive to the device detection geometry," *Biomed. Opt. Express* **3**, 1086–1100 (2012).
26. E. L. Hull, M. G. Nichols, T. H. Foster, "Quantitative broadband near-infrared spectroscopy of tissue-simulating phantoms containing erythrocytes," *Phys. Med. Biol.* **43**, 3381 (1998).
27. V. O. Korhonen *et al.*, "Light propagation in NIR spectroscopy of the human brain," *IEEE J. Sel. Top. Quantum Electron.* **20**, 1–10 (2014).

28. T. Myllylä, A. Popov, V. Korhonen, A. Bykov, M. Kinnunen, "Optical sensing of a pulsating liquid in a brain-mimicking phantom," *Proc. SPIE* **8799**, 87990X (2013).
29. H. S. S. Sorvoja, T. S. Myllylä, M. Y. Kirillin, E. A. Sergeeva, R. A. Myllylä, A. A. Elseoud, J. Nikkinen, O. Tervonen, V. Kiviniemi, "Non-invasive, MRI-compatible fibreoptic device for functional near-IR reflectometry of human brain," *Quantum Electron.* **40**, 1067 (2010).
30. E. Okada, M. Firbank, M. Schweiger, S. R. Arridge, M. Cope, D. T. Delpy, "Theoretical and experimental investigation of near-infrared light propagation in a model of the adult head," *Appl. Opt.* **36**, 21–31 (1997).
31. V. V. Tuchin, *Tissue Optics: Light Scattering Methods and Instruments for Medical Diagnosis*, SPIE Press (2007).
32. M. Firbank, M. Hiraoka, M. Essenpreis, D. T. Delpy, "Measurement of the optical properties of the skull in the wavelength range 650–950 nm," *Phys. Med. Biol.* **38**, 503–510 (1993).
33. A. N. Bashkatov, E. A. Genina, V. I. Kochubey, V. V. Tuchin, "Optical properties of human skin, subcutaneous and mucous tissues in the wavelength range from 400 to 2000 nm," *J. Phys. Appl. Phys.* **38**, 2543–2555 (2005).
34. P. van der Zee, M. Essenpreis, D. T. Delpy, "Optical properties of brain tissue," *Proc. SPIE* **1888**, 454–465 (1993).
35. P. van der Zee, "Measurement and modelling of the optical properties of human tissue in the near infrared," PhD Thesis, University College London, London (1992).
36. J. W. Pickering, S. A. Prahl, N. Van Wieringen, J. F. Beek, H. J. Sterenborg, M. J. Van Gemert, "Double-integrating-sphere system for measuring the optical properties of tissue," *Appl. Opt.* **32**, 399–410 (1993).
37. S. A. Prahl, M. J. van Gemert, A. J. Welch, "Determining the optical properties of turbid media by using the adding–doubling method," *Appl. Opt.* **32**, 559–568 (1993).
38. J. Fu, G. Quan, H. Gong, "A simple method for prediction of the reduced scattering coefficient in tissue-simulating phantoms," *J. Innov. Opt. Health Sci.* **3**, 53–59 (2010).
39. H. Kang, M. L. Clarke, S. H. Lacerda, A. Karim, L. F. Pease, J. Hwang, "Multimodal optical studies of single and clustered colloidal quantum dots for the long-term optical property evaluation of quantum dot-based molecular imaging phantoms," *Biomed. Opt. Express* **3**, 1312–1325 (2012).
40. Q. Wang, K. Shastri, T. J. Pfefer, "Experimental and theoretical evaluation of a fiber-optic approach for optical property measurement in layered epithelial tissue," *Appl. Opt.* **49**, 5309–5320 (2010).
41. T. Moffitt, Y.-C. Chen, S. A. Prahl, "Preparation and characterization of polyurethane optical phantoms," *J. Biomed. Opt.* **11**, 041103 (2006).
42. A. P. Popov, A. V. Priezzhev, R. Myllylä, "Effect of glucose concentration in a model light-scattering suspension on propagation of ultrashort laser pulses," *Quantum Electron.* **35**, 1075 (2005).
43. E. Alarousu, J. T. Hast, M. T. Kinnunen, M. Y. Kirillin, R. A. Myllyla, J. Plucinski, A. P. Popov, A. V. Priezzhev, T. Prykari, J. Saarela, Z. Zhao, "Noninvasive glucose sensing in scattering media using OCT, PAS, and TOF techniques," *Proc. SPIE* **5474**, 33–41 (2004).
44. M. T. Kinnunen, A. P. Popov, J. Plucinski, R. A. Myllyla, A. V. Priezzhev, "Measurements of glucose content in scattering media with time-of-flight technique: Comparison with Monte Carlo simulations," *Proc. SPIE* **5474**, 181–191 (2004).
45. A. P. Popov, A. V. Bykov, S. Toppari, M. Kinnunen, A. V. Priezzhev, R. Myllyla, "Glucose sensing in flowing blood and intralipid by laser pulse time-of-flight and optical coherence tomography techniques," *IEEE J. Sel. Top. Quantum Electron.* **18**, 1335–1342 (2012).
46. H. J. van Staveren, C. J. Moes, J. van Marie, S. A. Prahl, M. J. van Gemert, "Light scattering in Intralipid-10% in the wavelength range of 400–1100 nm," *Appl. Opt.* **30**, 4507–4514 (1991).
47. S. T. Flock, S. L. Jacques, B. C. Wilson, W. M. Star, M. J. van Gemert, "Optical properties of Intralipid: A phantom medium for light propagation studies," *Lasers Surg. Med.* **12**, 510–519 (1992).
48. A. Agrawal, S. Huang, A. W. H. Lin, M.-H. Lee, J. K. Barton, R. A. Drezek, T. J. Pfefer, "Quantitative evaluation of optical coherence tomography signal enhancement with gold nanoshells," *J. Biomed. Opt.* **11**, 041121 (2006).
49. D. M. de Bruin, R. H. Bremmer, V. M. Kodach, R. de Kinkelder, J. van Marle, T. G. van Leeuwen, D. J. Faber, "Optical phantoms of varying geometry based on thin building blocks with controlled optical properties," *J. Biomed. Opt.* **15**, 025001 (2010).
50. J. Pluciński, A. F. Frydrychowski, J. Kaczmarek, W. Juzwa, "Theoretical foundations for noninvasive measurement of variations in the width of the subarachnoid space," *J. Biomed. Opt.* **5**, 291–299 (2000).
51. P. Moilanen, Z. Zhao, P. Karppinen, T. Karppinen, V. Kilappa, J. Pirhonen, R. Myllylä, E. Haeggström, J. Timonen, "Photo-acoustic excitation and optical detection of fundamental flexural guided wave in coated bone phantoms," *Ultrasound Med. Biol.* **40**, 521–531 (2014).

52. A. P. Popov, S. Haag, M. Meinke, J. Lademann, A. V. Priezzhev, R. Myllylä, "Effect of size of TiO_2 nanoparticles applied onto glass slide and porcine skin on generation of free radicals under ultraviolet irradiation," *J. Biomed. Opt.* **14**, 1011 (2009).
53. A. Sarkar, A. Shchukarev, A.-R. Leino, K. Kordas, J.-P. Mikkola, P. O. Petrov, E. S. Tuchina, A. P. Popov, M. E. Darvin, M. C. Meinke, J. Lademann, V. V. Tuchin, "Photocatalytic activity of TiO_2 nanoparticles: Effect of thermal annealing under various gaseous atmospheres," *Nanotechnology* **23**, 475711 (2012).